



$^{40}\text{Ar}/^{39}\text{Ar}$ dating of a hydrothermal pegmatitic buddingtonite–muscovite assemblage from Volyn, Ukraine

Gerhard Franz¹, Masafumi Sudo², and Vladimir Khomenko³

¹Institut für Angewandte Geowissenschaften, Technische Universität Berlin, Berlin, 10587, Germany

²Institut für Geowissenschaften, Universität Potsdam, Potsdam, 14476, Germany

³Semenenko Institute of Geochemistry, Mineralogy, and Ore Formation, National Academy of Sciences of Ukraine, pr. Palladina 34, Kiev, 03680 Ukraine

Correspondence: Gerhard Franz (gefra548@gmail.com)

Received: 31 August 2021 – Revised: 1 December 2021 – Accepted: 9 December 2021 – Published: 12 January 2022

Abstract. We determined $^{40}\text{Ar}/^{39}\text{Ar}$ ages of buddingtonite, occurring together with muscovite, with the laser-ablation method. This is the first attempt to date the NH_4 -feldspar buddingtonite, which is typical for sedimentary–diagenetic environments of sediments, rich in organic matter, or in hydrothermal environments, associated with volcanic geyser systems. The sample is a hydrothermal breccia, coming from the Paleoproterozoic pegmatite field of the Korosten Plutonic Complex, Volyn, Ukraine. A detailed characterization by optical methods, electron microprobe analyses, backscattered electron imaging, and IR analyses showed that the buddingtonite consists of euhedral-appearing platy crystals of tens of micrometers wide, 100 or more micrometers in length, which consist of fine-grained fibers of $\leq 1\ \mu\text{m}$ thickness. The crystals are sector and growth zoned in terms of $\text{K-NH}_4\text{-H}_3\text{O}$ content. The content of K allows for an age determination with the $^{40}\text{Ar}/^{39}\text{Ar}$ method, as well as in the accompanying muscovite, intimately intergrown with the buddingtonite. The determinations on muscovite yielded an age of $1491 \pm 9\ \text{Ma}$, interpreted as the hydrothermal event forming the breccia. However, buddingtonite apparent ages yielded a range of $563 \pm 14\ \text{Ma}$ down to $383 \pm 12\ \text{Ma}$, which are interpreted as reset ages due to Ar loss of the fibrous buddingtonite crystals during later heating. We conclude that buddingtonite is suited for $^{40}\text{Ar}/^{39}\text{Ar}$ age determinations as a supplementary method, together with other methods and minerals; however, it requires a detailed mineralogical characterization, and the ages will likely represent minimum ages.

1 Introduction

Buddingtonite, the monoclinic (space group $P2_1/m$) ammonium feldspar ($\text{NH}_4\text{AlSi}_3\text{O}_8$), occurs in two geological settings: in igneous rocks in hydrothermal environments, such as volcanic geyser fields (Erd et al., 1964), and in sediments rich in organic matter (OM), such as coal seams (Dai et al., 2018), oil shales (e.g., Loughnan et al., 1983; Patterson et al., 1988), phosphorites (Gulbrandsen, 1974), black shales (e.g., Harlov et al., 2001), and sandstones (Ramseyer et al., 1993). It frequently occurs together with clay minerals such as illite or montmorillonite with a high content of NH_4 (e.g., Erd et al., 1964; Voncken et al., 1993) and is the source of molecular N_2 in natural gases (Krooss et al., 2005). Buddingtonite is often characterized as a “nondescript and amor-

phous” appearing mineral (e.g., Pampeyan, 2010), mostly fine-grained or in micrometer-wide rims on K-feldspar. It is a trace component in pegmatitic feldspar (Solomon and Rossman, 1988) but forms continuous solid solution with K-feldspar (Pöter et al., 2007; Svenson et al., 2008), which might be formed either due to partial replacement of igneous or detrital K-feldspar or together with authigenic K-feldspar. Analogous to the K-feldspar–buddingtonite solid solution, there exists a muscovite–tobelite solid solution $\text{K}_4\text{AlSi}_3\text{O}_{10}(\text{OH})_2\text{-NH}_4\text{AlSi}_3\text{O}_{10}(\text{OH})_2$, and K– NH_4 -bearing micas and feldspar frequently occur together. The K content in buddingtonite would allow applying the K–Ar decay system to date the formation of such buddingtonite–K-feldspar solid solutions, which would give valuable time information for a diagenetic or a hydrothermal event. In addi-

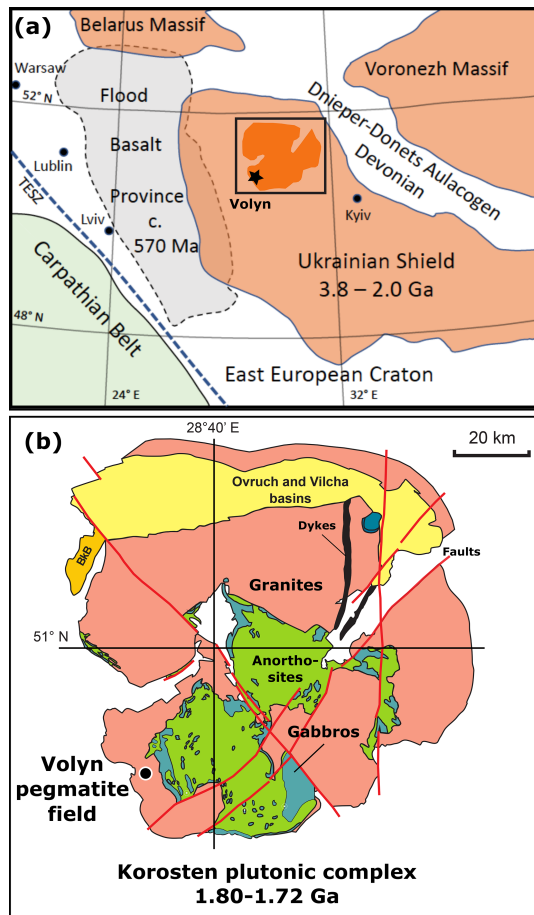


Figure 1. (a) Sample locality of the Volyn pegmatite field near Khoroshiv (former Volodarsk-Volynsky), Ukrainian Shield of the East European Craton, bound by the Trans-European Suture Zone (TESZ) and the Carpathian Belt. The Archean to Paleoproterozoic Ukrainian Shield partly overlaps with the Ediacaran Volyn Flood Basalt Province in the west and is bound in the northeast by the Devonian Dnieper–Donetsk Aulacogen. Square indicates position of (b), showing the Korosten plutonic complex, with the Volyn pegmatite field on its southwestern border. In the north, the pluton is covered by sediments of the Ovruch and Vilcha basins, and in the west by sediments of the Bilokorowychi basin (BkB); compiled from Shumlyanskyy et al. (2016, 2017).

tion, the common occurrence of buddingtonite in sediments rich in OM gives a minimum age for the fossil organisms which produced the OM. To our knowledge, no attempts have been made to date buddingtonite, and here we present our results from a sample with a hydrothermal buddingtonite–muscovite association, formed in the Paleoproterozoic Volyn pegmatite field, Ukraine (Fig. 1).

2 Sample and methods

2.1 Sample description and geological background

The Volyn pegmatite field at Khoroshiv (former Volodarsk-Volynsky) is situated in the northwestern part of the Precambrian Ukrainian Shield (Fig. 1a). The pegmatites are associated with the Paleoproterozoic Korosten anorthosite–mangerite–charnockite–granite plutonic complex in the border facies of rapakivi-type granites (Fig. 1b). A summary of descriptions of these pegmatites is found in Lyckberg et al. (2009, 2019, and references therein). Intrusion ages of the pluton range from 1.84 to 1.72 Ga (Shumlyanskyy et al., 2017), and the ages of the granite (1766 ± 3 Ma) and pegmatite (1760 ± 3 Ma) near to Volyn were determined on zircon by U–Pb dating with secondary ion mass spectrometry (SIMS; Shumlyanskyy et al., 2021).

The rock sample (Fig. 2) was collected in 2008 at the waste dump at Khoroshiv. It is a pegmatite breccia, cemented by opal, and contains fragments of pegmatitic minerals (mainly alkali-feldspar, quartz) and a pseudomorph after pegmatitic beryl, described in detail in Franz et al. (2017). This pseudomorph consists of muscovite + buddingtonite together with Be-mineral bertrandite and minor euclase (and other rare minerals). The simplified formation reaction is $4 \text{beryl} + 4 \text{K-feldspar} + 7 \text{H}_2\text{O} = 3 \text{bertrandite} + 4 \text{muscovite} + 18 \text{quartz}$. It also contains organic matter (OM), which shows different stages of oxygenation, accompanied by loss of N. Dissolved N as NH_4^+ transformed K-feldspar into buddingtonite–K-feldspar solid solutions and partly transformed muscovite into tobelite. The primary organic matter was found in miarolitic cavities of the pegmatites as fibrous fossils consisting of kerite (highly mature OM; Gorlenko et al., 2000; Zhmur, 2003; Franz et al., 2017). The cementing opal with a macroscopic black color is characterized by brown pigmentation in thin section, which is due to carbon hydrates included in the opal (Franz et al., 2017).

Three blocks of approximately 1 cm^2 in size from the cut surface of the pseudomorph sample V2008 (Fig. 2) were polished for investigation by back scattered electron (BSE) images in the electron microprobe (EMPA) at ZE electron microscopy, TU Berlin. Two blocks were finally used for analyses: one with a large amount of buddingtonite, and the other with abundant muscovite. BSE images are provided in Figs. 3 and 4.

The textural context of muscovite and buddingtonite is critical for the interpretation of the results of the $^{40}\text{Ar}/^{39}\text{Ar}$ dating and is therefore described here, based on previous investigations of this sample (see also Franz et al., 2017, for more BSE images of textures). Muscovite is lath-shaped in randomly oriented crystals or packages of crystals of up to $100 \mu\text{m}$ perpendicular to $\{001\}$ and several hundreds of micrometers long (Figs. 3, 5a, b, c). They partly enclose buddingtonite (Fig. 5b) and in areas close to buddingtonite, a lower BSE contrast indicates a significant

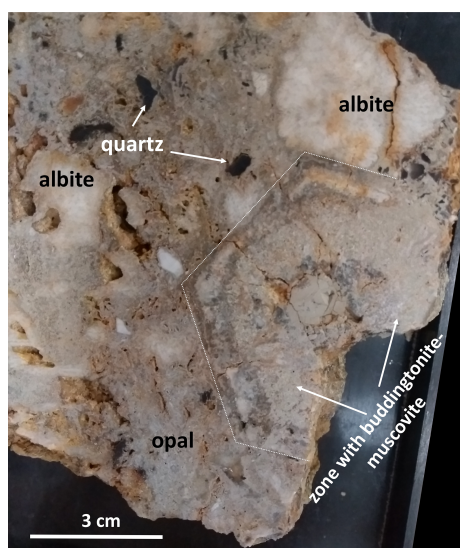


Figure 2. Photograph of the hand specimen (cut surface) with the investigated pseudomorph (outlined) of bertrandite + muscovite + buddingtonite ± euclase in a breccia of pegmatitic minerals, cemented by opal.

NH_4 -(tobelite) component (Fig. 5c). An average analysis is $(\text{NH}_4)_{0.29}\text{K}_{1.76}\text{Na}_{0.007}\text{Ca}_{0.003}\text{Al}_{3.555}\text{Fe}_{0.219}^{3+}\text{Mg}_{0.035}\text{Mn}_{0.004}\text{Ti}_{0.003}[\text{Si}_{6.685}\text{Al}_{1.315}\text{O}_{20}|\text{F}_{0.461}(\text{OH})_{1.539}]$; the maximum tobelite component is 25 mol %. X-ray mapping confirms the replacement of K by NH_4 (see Fig. 5 in Franz et al., 2017). Crystals without detectable tobelite component can be high in F, in some analyses with > 50 mol % of the F-muscovite endmember, concentrated mostly in the core of crystals. Beryllium, B, and Li were checked by SIMS and were found to be on the parts-per-million level. Analysis with high Si indicates intergrowths below the resolution of the EMPA with a silica phase like opal/tridymite (based on X-ray diffraction investigation).

Buddingtonite occurs dominantly in a network of euhedral, platy-appearing crystals (Fig. 4), together with F-muscovite and opal (Fig. 5a), and replacing K-feldspar (Fig. 5d) and albite. Replacement of K-feldspar results in oriented overgrowths. Buddingtonite appears as crystals several tens of micrometers large with typical sector zoning (Fig. 5d, e, f). Important for the interpretation of the $^{40}\text{Ar}/^{39}\text{Ar}$ dating results is that euhedral-appearing crystals consist of micrometer-sized fibers indicated by a slightly different extinction position in thin section. Solid solution of dominantly NH_4 –K creates a strong variation in BSE contrast. There are also intermediate euhedral-fibrous textures (Fig. 5e) with clear zoning in the core, extending outward into fibrous aggregates. Most of the crystals are sector zoned (Fig. 6; from Franz et al., 2017, with permission of the Mineralogical Society of America).

Buddingtonite is not stable under a focused beam (Fig. 5d). An average of 13 analyses (beam

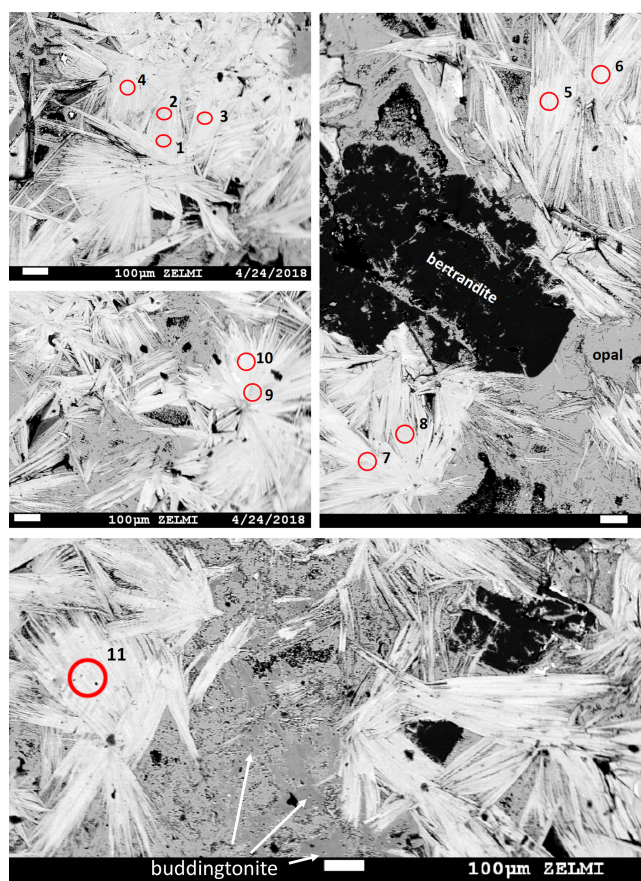


Figure 3. BSE images of polished pieces of sample V2008b, of the muscovite-rich part of the pseudomorph, prepared for irradiation. Numbered circles indicate sites of laser-ablation spots (see Table 1; test runs 1, 2, and 3 are not marked). White lath-shaped crystals are muscovite; difference in BSE contrast is due to a small tobelite component in slightly greyer crystals, together with bertrandite (black), buddingtonite, and opal (gray). Scale bar is 100 μm in all images.

diameter of 15 μm , which averages over heterogeneities within a crystal) yields a formula $\text{Na}_{0.02}\text{K}_{0.20}(\text{NH}_4)_{0.63}\text{H}_3\text{O}_{0.15}[\text{Si}_{3.03}\text{Al}_{1.01}\text{Fe}_{0.01}^{3+}\text{O}_8]$ but with a strong variation for K between 0.09 and 0.27 cations per formula unit (cpfu) and 0.28 and 0.96 cpfu for NH_4 . X-ray mapping (WDS) of the major components (Figs. 4 and 5 in Franz et al., 2017) and BSE images (Fig. 5d, e, f) highlight the zoning. The amount of H_3O is estimated from $1.00 - (\text{Na} + \text{K} + \text{NH}_4)$; the presence of “water”, either as H_2O or H_3O^+ , was verified by infrared spectroscopy. We concluded that from crystal to crystal and within the crystals the amount of substitution NH_4 –Na–K in combination with H_3O differs. Trace elements Ti, Mg, Mn, Ca, Cs, and Rb are always close to or below the detection limit (≤ 0.01 wt % oxide). A “water” content has been predicted to occur in buddingtonite and is discussed by Barker (1964), Laricheva et al. (1993), and Harlov et al. (2001), and this “water”

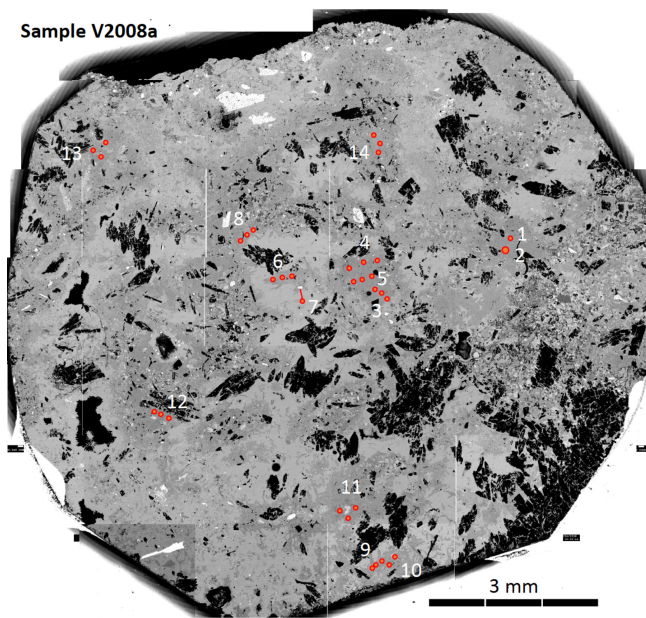


Figure 4. BSE mosaic image of sample V2008a: polished piece of the pseudomorph, prepared for irradiation, rich in buddingtonite (dark gray BSE contrast, compared to light gray BSE contrast of opal). Crystals with black BSE contrast are bertrandite, and crystals with white BSE contrast are alkali feldspar. Numbers refer to analysis number in Table 1 (test runs 1 and 2 not marked), and red spots indicate laser-ablation spots. Three shots were used for one analysis except for analysis 7, a relict K-feldspar.

content in combination with NH_4 might be the reason for the sensitivity of the crystals to the electron beam.

Another observation from the pegmatites and the breccia with the pseudomorph, critical for the interpretation of the ages, is the occurrence of black opal (Gigashvili and Kalyuzhnyi, 1969). This type of opal contains carbohydrates (Franz et al., 2017), which cause the black appearance, with a brown color in thin section. The carbohydrates originate from decaying OM (Fig. 7a), and the opal is found also in cracks within the OM. These textural observations indicate that it is one of the last precipitates in the breccia. Furthermore, it completely encloses bertrandite (Fig. 7b) and buddingtonite (Fig. 7c). It is characterized by zonal BSE contrast (Fig. 7b, d), probably caused by different water and carbohydrate content, and is also surrounding muscovite with parts rich in tobelite component (Figs. 6e, 4b). It also contains small ($\leq 1\ \mu\text{m}$) inclusions of other minerals, possibly Al-silicates and Ca-sulfate (Fig. 7f; energy dispersive spectroscopy – EDS – spectrum). Opal shows strong zoning where the dark areas (lower average atomic weight number) are assumed to be opal-A with a higher content of H_2O than the light areas, which is opal-CT (cf. Day and Jones, 2008). The common transition from opal-A (amorphous) to quartz goes via opal-CT (see Graetsch, 1994).

2.2 Methods

The $^{40}\text{Ar}/^{39}\text{Ar}$ analyses have been performed at the $^{40}\text{Ar}/^{39}\text{Ar}$ geochronology laboratory in the University of Potsdam. Samples were prepared as thick sections, and the in situ analyses with Nd-YAG UV pulse laser were done following the BSE images of the surfaces. The system of the in situ analyses with a Micromass 5400 noble gas mass spectrometer was the same as described in Halama et al. (2014). Neutron activation of the samples was performed at the CLICIT (Cadmium-Lined In-Core Irradiation Tube) facility of Oregon State TRIGA Reactor (OSTR), USA. Samples were irradiated for 4 h together with the neutron flux monitoring mineral, Fish Canyon Tuff sanidine prepared at the Geological Survey of Japan (27.5 Ma; Uto et al., 1997; Ishizuka, 1998; Lanphere and Baadsgaard, 2001), and the salts of K_2SO_4 and CaF_2 for correction of interference. The actual analyses were conducted by MassSpec software developed by Alan Deino at Berkeley Geochronology Center, USA, and the $^{40}\text{Ar}/^{39}\text{Ar}$ age calculation was done following Uto et al. (1997). The decay constants of ^{40}K ($\lambda(^{40}\text{K}_{\beta^-})$: $4.962 \times 10^{-10}\ \text{yr}^{-1}$; $\lambda(^{40}\text{K}_e) + \lambda'(^{40}\text{K}_e)$: $0.581 \times 10^{-10}\ \text{yr}^{-1}$) and the value of atmospheric $^{40}\text{Ar}/^{36}\text{Ar}$ (295.5) follow Steiger and Jäger (1977). The spot sizes of the ablated area used were $50\ \mu\text{m}$ for muscovite in sample V2008b and $100\ \mu\text{m}$ for buddingtonite and K-feldspar in sample V2008a.

3 Results

Results of Ar isotope measurements are given with relative Ar isotopic ratios in Table 1. All the errors obtained by $^{40}\text{Ar}/^{39}\text{Ar}$ dating (Table 1, Fig. 7) are indicated as 1σ errors. For buddingtonite, we obtained 11 ablation spots. One spot was measured on a small grain of relict K-feldspar, enclosed in buddingtonite. The result of this measurement confirms a high age (930 Ma), interpreted as a reset age from the igneous crystallization/cooling event, which should be near 1.7 Ga. For muscovite we had obtained eight ablation spots, which show a restricted range of calculated ages varying from 1439 ± 22 to 1545 ± 28 Ma, and allowing for the calculation of a weighted mean age of 1491 ± 9 Ma (Fig. 8). To evaluate possible excess ^{40}Ar we plotted the normal isochron diagrams ($^{40}\text{Ar}/^{36}\text{Ar}$ vs. $^{39}\text{Ar}/^{36}\text{Ar}$) and the inverse isochron diagrams ($^{36}\text{Ar}/^{40}\text{Ar}$ vs. $^{39}\text{Ar}/^{40}\text{Ar}$) by assuming all the results have the common same age. Both isochron plots show similar ages compared to the obtained ages by each in situ analysis, and the estimated initial $^{40}\text{Ar}/^{36}\text{Ar}$ also agrees (within 2σ) with the atmospheric value. Therefore, the probability that muscovite contains excess ^{40}Ar is very small and does not significantly influence the actual obtained ages. Furthermore, Scibiorsky et al. (2021) report that excess ^{40}Ar is more common in metamorphic rocks than in igneous rocks and that one of the conditions for retaining excess Ar is a low permeabil-

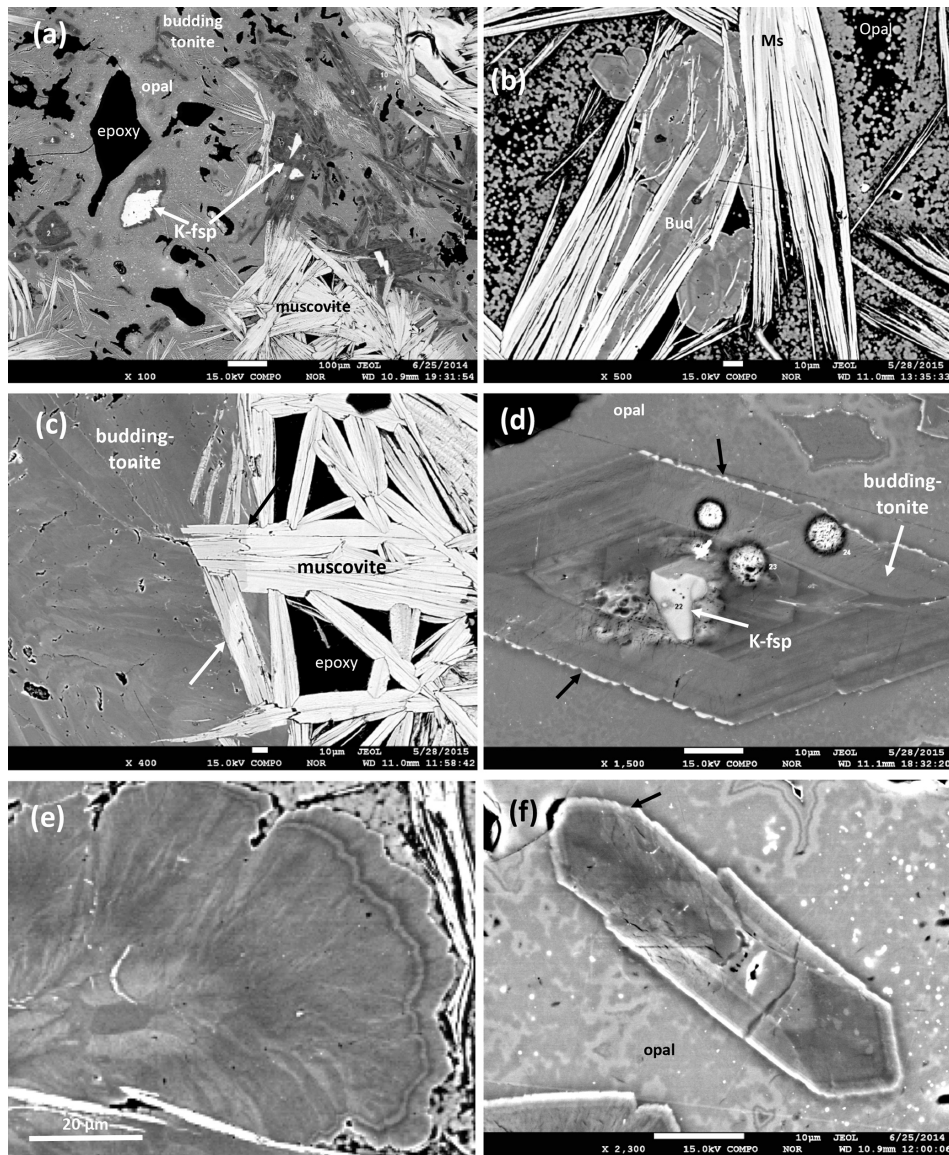


Figure 5. BSE images of the buddingtonite–muscovite assemblage. (a, b) Overview: lath-shaped crystals with white BSE contrast are muscovite, buddingtonite is dark gray, and opal is light gray. White crystals within buddingtonite are relict, igneous K-feldspar. Note large pore space, filled by epoxy. (c) Contact of muscovite to buddingtonite; arrows point to change in BSE contrast in muscovite, indicating a significant tobelite component. (d) Buddingtonite with sector zoning and relict K-feldspar in opal matrix. Black arrows point to enrichment of the K-feldspar component in the outermost rim. White, round dots are areas of beam damage due to analysis. (e) Outer part of an oscillatory zoned buddingtonite crystal; darker areas are rich in N and H_2O . Note fibrous character with individual fibers $\leq 1\ \mu\text{m}$. (f) Sector zoned crystal, approximately $10\ \mu\text{m}$ wide, with $< 1\ \mu\text{m}$ outgrowths at its tip (arrow). Small numbers in (a) and (d) refer to analyses published in Franz et al. (2017).

ity of the rocks, which prevents fluids carrying Ar to leave the rock, such as in eclogites and blueschists. However, the breccia was formed in the uppermost crust and has a high porosity; therefore it is unlikely that excess Ar (possibly produced in the K-rich surrounding pegmatites) was retained.

In contrast, the apparent buddingtonite ages show a wide range of much younger ages from 383 ± 12 to 563 ± 14 Ma, indicating significant resetting by Ar loss. The

age-probability curve is shown in Fig. 7. We also calculated $^{40}\text{Ar}/^{39}\text{Ar}$ ages with the recently proposed decay constants of ^{40}K by Renne et al. (2011), considering the comparison with Rb–Sr ages according to the method of Villa et al. (2015). The ages calculated with these decay constants are maximal 5 Myr older at 500 Ma and maximal 11 Myr older at 1500 Ma. The 1σ errors on all the $^{40}\text{Ar}/^{39}\text{Ar}$ ages indicated in this study are the external errors including the error on

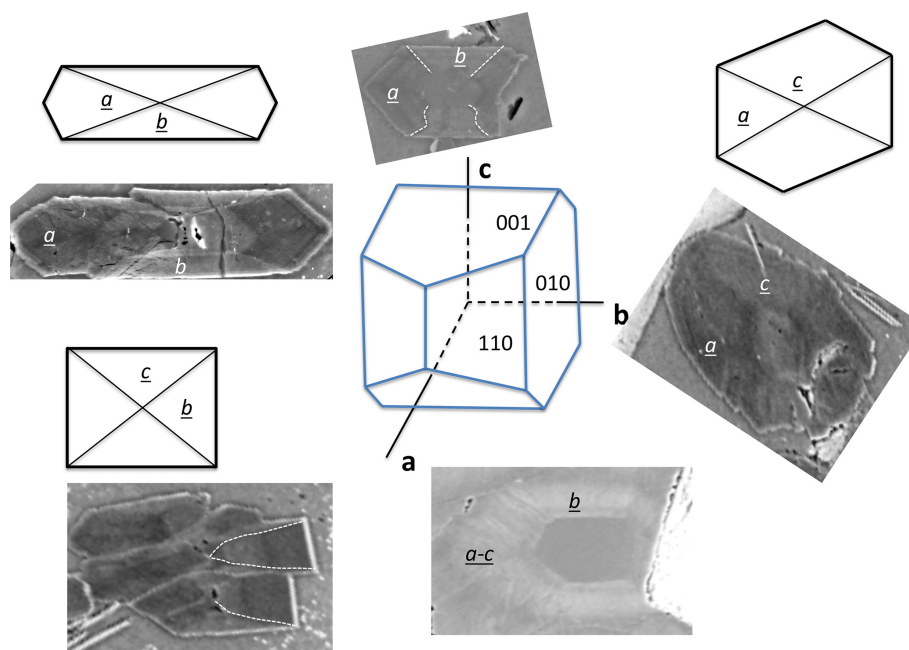


Figure 6. Schematic drawing of sector zoning in buddingtonite and corresponding BSE images. The a sectors and the core are enriched in NH_4 , and b and c sectors are K-rich and appear with brighter BSE contrast. Note the fibrous character of the euhedral-appearing crystals (from Franz et al., 2017; with permission of the Mineralogical Society of America).

the J value of 0.4 %. The $^{37}\text{Ar}/^{39}\text{Ar}$ values (Table 1) show that in the most of the analyses Ca-derived ^{37}Ar is insignificant; thus in most cases there were few special sources for Ca within the samples. No Ca minerals were found in the pseudomorph.

4 Discussion

The sample, with a high porosity partly filled with opal (Figs. 2, 4b), was collected from the waste dump, having been exposed to weathering conditions for several years. However, the EMPA showed a completely filled interlayer position of muscovite, and therefore we assume that leaching of K–Ar from muscovite was minor, and spots for laser ablation were always chosen in the central parts of the crystals. The eight spot analyses range from 1439 ± 22 to 1545 ± 28 Ma (Table 1). The mean calculated age of 1491 ± 9 Ma (Fig. 8b) is considered to be a geologically meaningful age. Closure temperature for the K–Ar system in muscovite is in the range of 300–400 °C (e.g., Rainers and Brandon, 2006), and since the formation temperature of the pseudomorph was ≤ 200 °C (Franz et al., 2017), the age of 1491 Ma is near to the crystallization age. It is known that in the absence of dynamic recrystallization – which is the case for the pseudomorph –, white mica preserves the Ar isotope record (Di Vincenzo et al., 2001). We do see, however, indications for fluid-induced reprecipitation of the muscovite by tobelite (Fig. 5b, c), and that these reactions strongly in-

fluence the Ar–Ar system is seen in muscovite, for example, by Naumenko-Dèzes et al. (2021). The influence on the muscovite ages by this replacement is discussed below in the context of the age data of buddingtonite.

The large time difference between crystallization of the pegmatites (1760 ± 3 Ma; Shumlyanskyy et al., 2021) of approximately 270 Ma indicates a hydrothermal event independent of the cooling stage of the pegmatite. Cooling of the pegmatite down to temperatures suitable for microorganisms is also required by the fact that the kerite fossils grew inside the miarolitic cavities.

However, the high F content of the muscovite with up to 50 mol % of the F endmember requires a fluid rich in F (Muñoz and Eugster, 1969), which likely originates from the pegmatitic environment, where topaz and fluorite are common (Lyckberg et al., 2009). This fluid, which circulated in the rocks during the hydrothermal event, also affected the OM; this degraded OM from the original kerite microfossils contains high concentrations of high field strength elements (e.g., ≤ 7 at. % Zr, ≤ 3 at. % Y, ≤ 1.25 at. % U; Franz et al., 2017), and we conclude that the fluid was able to dissolve Zr minerals and others. Fluid inclusion studies also point to a high CO_2 content (Voznyak et al., 2012). An HF-bearing fluid must have been also responsible for a large amount of silica, which precipitated as carbohydrate-bearing opal and cemented the breccia.

Textural information on the close association of muscovite and buddingtonite indicate that both minerals were formed together in a single hydrothermal event, with precipitation of

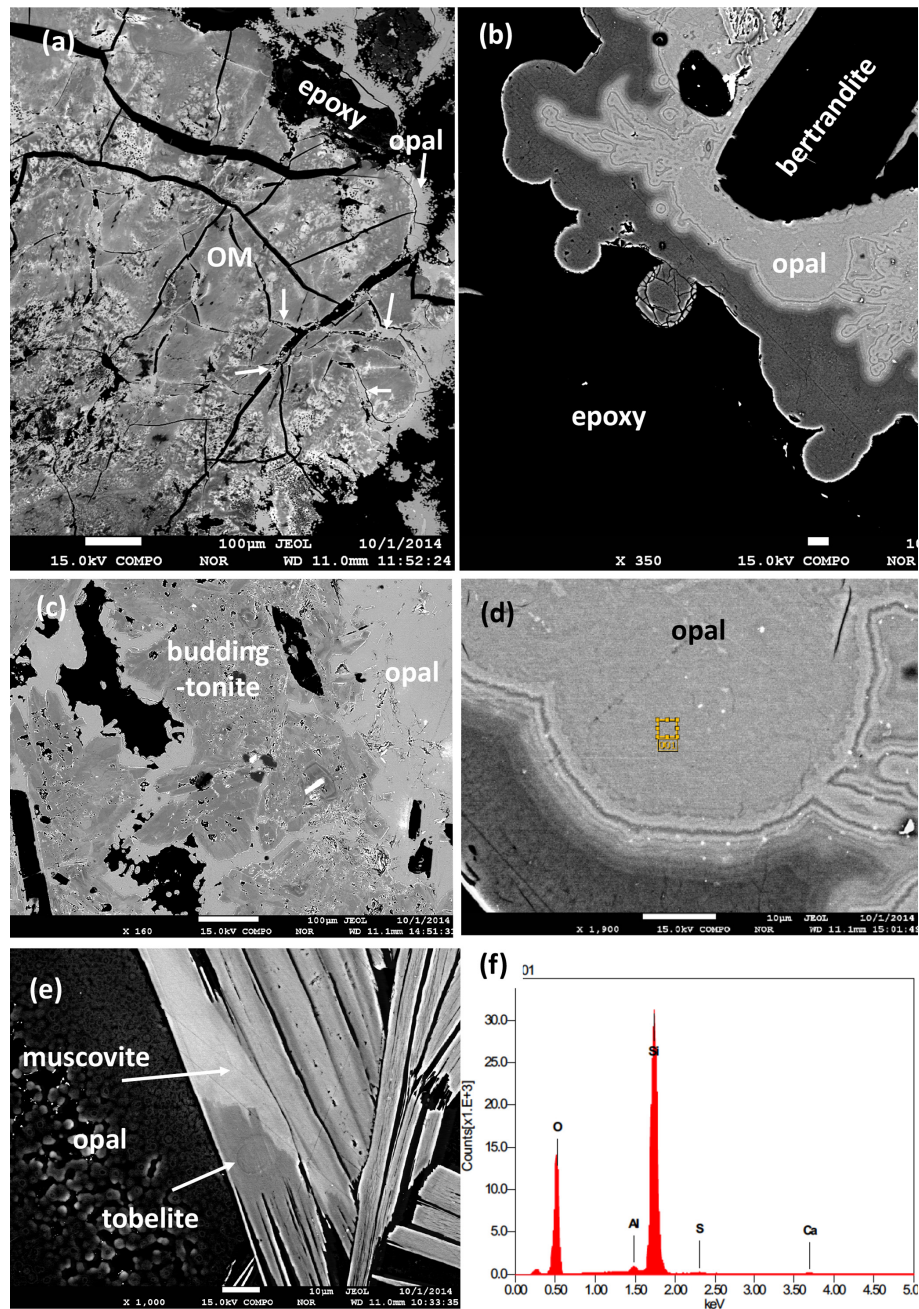


Figure 7. BSE images of black opal from the pseudomorph. (a) Organic matter with differences in BSE contrast due to different content of Zr and other high field strength elements; opal (arrow) occurs in cracks and on the rim. (b) Zoned opal surrounding bertrandite. (c) Opal surrounding buddingtonite. (d) Detail of zoned opal with nanometer-sized inclusions (bright contrast). Rectangle indicates position of EDS analysis. (e) Opal next to muscovite with different BSE contrast due to different tobelite component. (f) EDS analysis of black opal with traces of Al, S, and Ca.

black opal as the last precipitate (Fig. 7), enclosing buddingtonite and muscovite, and also in cracks of the degraded organic matter. The textures of muscovite, replaced by tobelite, and the growth zoning in buddingtonite (Fig. 5d, e) and in opal (Fig. 7b, d) clearly indicate that the fluid composition changed during the pseudomorph formation, starting with

F-dominated K-rich fluids producing pure F-muscovite, followed by alternating NH_4 -rich and K-rich compositions producing oscillatory growth zones in buddingtonite (Fig. 5e) and ending with a late K-rich fluid (producing some outer K-rich zones in buddingtonite; Fig. 5d).

Table 1. Results of Ar isotopic ratios' measurements.

Analysis no.	$^{40}\text{Ar}/^{39}\text{Ar}$	$^{37}\text{Ar}/^{39}\text{Ar}$	$^{36}\text{Ar}/^{39}\text{Ar}$ ($\times 10^{-3}$)	$^{37}\text{Ar}_{\text{Ca}}/^{39}\text{Ar}_{\text{K}}$	$^{40}\text{Ar}^*$ (%)	$^{40}\text{Ar}^*/^{39}\text{Ar}_{\text{K}}$	Age ($\pm 1\sigma$) (Ma)
V2008a buddingtonite							
1119-03	595 \pm 11	0.0 \pm 1.1	1085 \pm 40	0.0012	46.13	275 \pm 13	439 \pm 18
1119-04	577 \pm 10	0.0 \pm 1.5	1048 \pm 39	0.0012	46.32	267 \pm 12	429 \pm 18
1119-05	788 \pm 14	0.0 \pm 2.5	1574 \pm 57	0.0018	41.01	323 \pm 18	507 \pm 24
1119-06	850 \pm 13	0.0 \pm 1.8	1833 \pm 46	0.0014	36.30	309 \pm 14	487 \pm 19
1119-08	450 \pm 8	0.1 \pm 1.4	545 \pm 20	0.1053	64.19	289 \pm 8	459 \pm 11
1119-09	416 \pm 9	0.0 \pm 1.3	334 \pm 14	0.0011	76.29	317 \pm 8	499 \pm 12
1119-10	360 \pm 6	1.9 \pm 1.1	423 \pm 22	1.8917	65.38	236 \pm 8	383 \pm 12
1119-11	447 \pm 8	1.8 \pm 1.1	653 \pm 16	1.8011	56.88	255 \pm 7	411 \pm 10
1119-12	669 \pm 12	0.0 \pm 1.6	1071 \pm 35	0.0016	52.70	353 \pm 12	547 \pm 17
1119-13	832 \pm 14	3.3 \pm 2.0	1584 \pm 31	3.3479	43.76	365 \pm 11	563 \pm 14
1119-14	385 \pm 6	2.1 \pm 1.2	341 \pm 14	2.0788	73.90	285 \pm 7	454 \pm 10
V2008a K-feldspar							
1119-07	1751 \pm 96	0.0 \pm 23.7	3551 \pm 259	0.0159	40.05	701 \pm 82	961 \pm 87
V2008b muscovite							
1118-04	1437 \pm 33	0.0 \pm 2.7	555 \pm 72	0.0027	88.59	1273 \pm 37	1484 \pm 29
1118-05	1501 \pm 34	0.0 \pm 3.1	841 \pm 61	0.0022	83.46	1253 \pm 34	1468 \pm 28
1118-06	1657 \pm 35	0.0 \pm 3.3	1039 \pm 70	0.0023	81.47	1350 \pm 36	1545 \pm 28
1118-07	1684 \pm 32	0.0 \pm 3.6	1250 \pm 67	0.0023	78.06	1314 \pm 33	1517 \pm 26
1118-08	1411 \pm 29	2.5 \pm 2.4	446 \pm 52	2.4951	90.67	1281 \pm 31	1491 \pm 25
1118-09	1449 \pm 33	0.0 \pm 2.2	407 \pm 65	0.0026	91.71	1329 \pm 36	1528 \pm 28
1118-10	1409 \pm 26	4.0 \pm 2.1	662 \pm 49	4.0564	86.13	1217 \pm 27	1439 \pm 22
1118-11	1404 \pm 31	1.7 \pm 1.9	468 \pm 47	1.6649	90.16	1267 \pm 32	1480 \pm 26

$^{40}\text{Ar}^*$ = radiogenic ^{40}Ar . J value for sample V2008a = $(1.004 \pm 0.004) \times 10^{-3}$; J value for V2008b = $(1.003 \pm 0.004) \times 10^{-3}$; 1σ errors include an error of J value (0.4%) and thus are external errors.

However, the coeval muscovite–buddingtonite formation could not be confirmed by the age determination. Apparent ages of buddingtonite are much younger, with a large spread between 383 ± 12 and 563 ± 14 Ma (Table 1; Fig. 8a), which is likely an effect of resetting due to Ar loss. In general, Ar loss from feldspar can occur via volume diffusion, by adjustment of the microstructure of the feldspar crystal lattice and its chemical composition to ambient low pressure-temperature conditions different from those of the crystallization conditions, by alteration during fluid–rock interaction and weathering, and by the recoil effect (e.g., Foland, 1994). We have pointed out above that the euhedral-appearing crystals actually consist of thin $\leq 1\ \mu\text{m}$ fibers (Figs. 4e, f, 5), and in such small crystallites volume diffusion is important. The recoil effect is also important in such small crystals and contributes to the scatter of the data. In addition, parallel to the fibers, subgrain-boundary diffusion likely was much faster than volume diffusion and effectively transported Ar out of the crystal; Wartho et al. (1999) suggested that diffusion along subgrain boundaries increases the diffusion rate by 4–5 orders of magnitude. Nevertheless, Mark et al. (2008) could show that Ar–Ar dating of

authigenic K-feldspar, which can be considered a close analogue to buddingtonite because of similar growth conditions, yielded geologically meaningful ages of diagenesis. They argue that the nature of subgrain boundaries in authigenic K-feldspar is significantly different from deuterically produced subgrain boundaries and that grain boundary diffusion was not effective in their samples. However, the buddingtonite subgrains are fibrillated, especially towards their outer parts, and we assume that these microtexturally different subgrain boundaries imply a different diffusion behavior than those of authigenic feldspar, as observed by Mark et al. (2008).

We also pointed out that the crystals are heterogeneous in terms of K–NH₄–H₂O (Figs. 4, 5), and re-equilibration between different sectors and zones would facilitate Ar diffusion out of the lattice (though to a minor degree since this must have occurred at temperatures $\leq \approx 200\ ^\circ\text{C}$, at which re-equilibration is very slow). The “water” content of the buddingtonite crystals might facilitate diffusion due to the easy proton exchange with surrounding oxygen, especially at higher temperature, that destabilizes the structure. The K–O and O–H₂O bond strengths are likely in the same order of magnitude, which is low considering the K–O stretch-

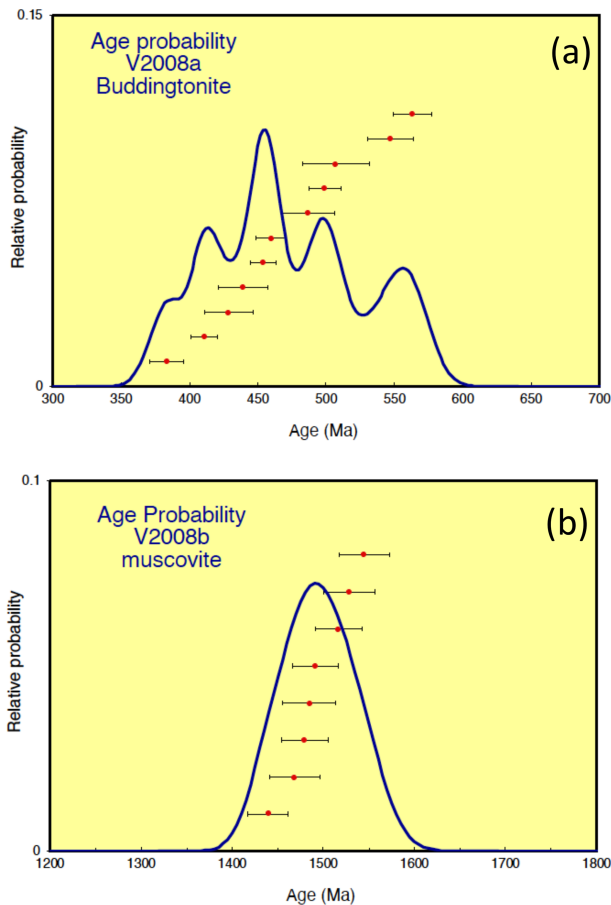


Figure 8. Results of $^{40}\text{Ar}/^{39}\text{Ar}$ dating for (a) buddingtonite and (b) muscovite. Whereas the muscovite ages show a restricted range varying from 1439 ± 22 to 1545 ± 28 Ma, allowing the calculation of a mean age of 1491 ± 9 Ma, the apparent buddingtonite ages ranging from 383 ± 12 to 563 ± 14 Ma indicate significant resetting of the ages by Ar loss (calculation with decay constants from Steiger and Jäger, 1977; calculations with decay constant for ^{40}K by Renne et al., 2011, yielded maximal 5 Myr older ages at 500 Ma and maximal 11 Myr older ages at 1500 Ma). The 1σ errors include an error of J value (0.4 %) and thus are external errors.

ing band near $\approx 100\text{--}120\text{ cm}^{-1}$. However, we are not aware of experimental data which would support this assumption. In addition, the thin fibers of buddingtonite might also be more susceptible to weathering and/or low-temperature hydrothermal fluid-mediated recrystallization than the larger muscovite crystals. In feldspar, dissolution–reprecipitation reactions are probably the most important processes for loss of Ar (Villa, 2014). In the microtexturally complicated buddingtonite samples with growth and sector zoning, Ar loss is likely also different from crystal to crystal. Note that in some crystals the core zones lack the fibrous character (Fig. 6), whereas rims are fibrous. In summary, we conclude that the apparent ages of buddingtonite are strongly reset and must be considered as minimum ages.

These reset ages can be explained in the framework of the regional geology of the Ukrainian Shield. The oldest apparent buddingtonite age of 563 ± 14 Ma is coeval with the effusive volcanism of Volyn flood basalts (Volyn LIP; Shumlyanskyy et al., 2016). Although the flood basalt province is in the order of 200 km towards the west from the pegmatite locality at Volyn (Fig. 1a), the formation of such a large volume of basalt over a distance from Poland and Belarus far into Ukraine must have been accompanied by an increased geothermal gradient effecting also the upper crust. A hydrothermal overprint at this time, at temperatures below the closure temperature of muscovite, is also seen in one of the zircon ages presented by Shumlyanskyy et al. (2021), which shows a discordia with a lower intercept at 550 ± 55 Ma. The further Phanerozoic geological development of the area is poorly restricted, but during the Devonian the Prypyat branch of the Dnieper–Donets paleorift (Shumlyanskyy et al., 2016) developed towards the northeast of the Ukrainian Shield (Fig. 1a). This process was likely accompanied by heating and provides a possible explanation for the youngest reset ages, down to 383 ± 12 Ma.

The age of a hydrothermal event near 1.5 Ga is new for Ukrainian Shield. This age might be correlated with similar apatite ages recently determined in the western Ukrainian Shield (Leonid Shumlyanskyy, personal communication, 2021). The heat source for this event is unknown; it could have been regional deformation, together with low-grade metamorphism. Gorokhov et al. (1981) determined Rb–Sr ages (illite and whole rock) for slightly metamorphosed sediments of the Belokorovichi formation (Ovruch Group), resting on the northern part of the Korosten pluton (Fig. 1b). Recalculated ages (Johannes Glodny, personal communication, 2021) with new decay constants (Villa et al., 2015) yielded for the illite fine fraction 1600 ± 31 Ma (recalculated from 1574 ± 31 Ma), and for the whole-rock isochron 1613 ± 75 Ma (recalculated from 1587 ± 74 Ma), such that the sediments experienced diagenetic and/or metamorphic overprinting possibly at ≈ 1.5 Ga, the formation age of the breccia. Detrital zircons, separated from metasediments surrounding and partly covering the Korosten Plutonic Complex in the northwestern–northeastern part, the so-called Volyn–Orsha depression (Shumlyanskyy et al., 2015) which extends from Lviv towards the northeast (Fig. 1a), yielded ages between 1500 and 1100 Ma (Polissya sandstone; Shumlyanskyy et al., 2015), indicating felsic magmatism in the source areas. These igneous events might also be correlated with the hydrothermal event in the Volyn area.

5 Summary and conclusions

The sedimentary–diagenetic or hydrothermally formed mineral buddingtonite is very likely suitable for minimum ages only, obtained via $^{40}\text{Ar}/^{39}\text{Ar}$ laser-ablation age determination. Before analysis, it requires a detailed characterization

by optical methods, electron microprobe analyses, backscattered electron imaging, and IR spectroscopic study. However, in combination with accompanying minerals such as muscovite in the reported case here, it allows for estimating the age framework of a sedimentary–diagenetic or a hydrothermal event. For the Volyn locality, it furthermore allows for estimating the age of the microfossils, which during decay produced the NH_4 content in the fluid to form buddingtonite (and the tobelite component in muscovite), as well as in the black opal; black opal is considered as the last precipitate in the breccia and the pseudomorph; therefore the OM must have been present before its precipitation. The zircon age of 1760 ± 3 Ma gives a clear maximum age for the fossils and the hydrothermal event at 1491 ± 9 Ma a minimum age. The coeval formation of buddingtonite with muscovite is based on textural arguments. A scenario with two hydrothermal events, a first one at 1491 ± 9 Ma followed by a second one near 563 ± 14 Ma, which was responsible for the decay of the microfossils and the production of NH_4 and buddingtonite formation is unlikely. It would mean that first a breccia with the beryl pseudomorph reaction was formed and then completely overprinted by a large amount of fluid circulation, dissolving F, Zr, and other high-field-strength elements from the pegmatites, creating a large pore space for the high amount of precipitation of opal. For such a strong event no indications were found, neither from the field geology nor in the geochemical description of the country rocks. We do not consider this as a likely interpretation, but the absolute minimum age of 563 ± 14 Ma clearly indicates a Precambrian age of the fossils.

The laser-ablation method for $^{40}\text{Ar}/^{39}\text{Ar}$ age determination has the advantage of in-situ-controlled determination but the disadvantage that stepwise heating is not possible. We would encourage more attempts for age determinations of buddingtonite, together with muscovite–illite from sedimentary–diagenetic rocks or hydrothermal deposits with the $^{40}\text{Ar}/^{39}\text{Ar}$ method, including analysis from mineral separates, which would be helpful to gain insight into sedimentary–diagenetic and hydrothermal processes.

Data availability. All data are presented in the article itself.

Sample availability. The sample is stored at the Mineralogische Sammlungen, Technische Universität Berlin. No IGSN has been assigned.

Author contributions. GF contributed to conceptualization, sampling, interpretation, and writing. MS contributed to the laser-ablation facility, measurement of the $^{40}\text{Ar}/^{39}\text{Ar}$ data, and writing. VK contributed to sampling, interpretation, and writing.

Competing interests. Gerhard Franz is a member of the managing committee of *European Journal of Mineralogy*. The other authors declare that they have no conflict of interest.

Disclaimer. Publisher's note: Copernicus Publications remains neutral with regard to jurisdictional claims in published maps and institutional affiliations.

Acknowledgements. We thank Leonid Shumlyanskyy (Perth) for helpful discussions about the geology of the Ukrainian Shield and valuable comments on an earlier version of the manuscript, Jörg Nissen from Zentraleinrichtung Elektronenmikroskopie (Berlin) for the BSE images, and Cordelia Lange (Berlin) for helping in sample preparation. Daniel Popov and Jens Hoppe are thanked for their critical and very helpful reviews.

Financial support. This research has been supported by Referat für Außenbeziehungen and the Open Access Publication Fund of TU Berlin, and by Deutsche Forschungsgemeinschaft (grant no. 436 UKR).

This open-access publication was funded by Technische Universität Berlin.

Review statement. This paper was edited by Dewashish Upadhyay and reviewed by Jens Hopp and Daniil Popov.

References

- Barker, D. S.: Ammonium in alkali feldspars, *Amer. Mineral.*, 49, 851–858, 1964.
- Dai, S., Xie, P., French, D., Ward, C. R., Graham, I. T., Yan, X., and Guo, W.: The occurrence of buddingtonite in super-high-organic-sulphur coals from the Yishan Coalfield, Guangxi, southern China, *Intern. J. Coal Geol.*, 195, 347–361, 2018.
- Day, R. and Jones, B.: Variations in water content in opal-A and opal-C-T from geyser discharge aprons, *J. Sed. Res.*, 78, 301–315, 2008.
- Di Vincenzo, G., Ghiribelli, B., Giorgetti, G., and Palmeri, R.: Evidence of a close link between petrology and isotope records: constraints from SEM, EMP, TEM and in situ $^{40}\text{Ar}/^{39}\text{Ar}$ laser analyses on multiple generations of white micas (Lanternman Range, Antarctica), *Earth. Planet. Sci. Lett.*, 192, 389–405, 2001.
- Erd, R. C., White, D. E., Fahey, J. J., and Lee, D. E.: Buddingtonite, an ammonium feldspar with zeolitic water, *Amer. Mineral.*, 49, 831–850, 1964.
- Foland, K. A.: Argon Diffusion in Feldspars, in: *Feldspars and their Reactions*, edited by: Parsons, I., NATO ASI Series (Series C: Mathematical and Physical Sciences), vol. 421, Springer, Dordrecht, https://doi.org/10.1007/978-94-011-1106-5_11, 1994.
- Franz, G., Khomenko, V., Vishnyevskyy, A., Wirth, R., Struck, U., Nissen, J., Gernert, U., and Rocholl, A.: Biologically mediated crystallization of buddingtonite in the Paleoproterozoic: Organic-

- igneous interactions from the Volyn pegmatite, Ukraine, *Amer. Mineral.*, 102, 2119–2135, 2017.
- Gigashvili, G. M. and Kalyuzhnyi, V. A.: Black opals from Volynian pegmatites, containing organic matter, *Doklady Akademii Nauk SSSR*, 186, 1154–1157, 1969 (in Russian).
- Gorlenko, V. M., Zhmur, S. I., Duda, V. I., Suzina, N. E., Osipov, G. A., and Dimitriev, V. V.: Fine structure of fossilized bacteria in Volyn kerite, *Orig. Life Evol. Biosph.*, 30, 567–577, 2000.
- Gorokhov, I. M., Clauer, N., Varshavskaya, E. S., Kutuyavin, E. P., and Drannik, A. S.: Rb-Sr ages of Precambrian sediments from the Ovruch mountain range, northwestern Ukraine (U.S.S.R.), *Precam. Res.*, 16, 55–65, 1981.
- Graetsch, H.: Structural characteristics of opaline and microcrystalline silica minerals, *Reviews Min. Geochem.*, 29, 209–232, 1994.
- Gulbrandsen, R. A.: Buddingtonite, ammonium feldspar, in the Phosphoria Formation, southeastern Idaho, *J. Res. US Geol. Surv.*, 2.6, 693–697, 1974.
- Halama, R., Konrad-Schmolke, M., Sudo, M., Marschall, H., and Wiedenbeck, M.: Effects of fluid-rock interaction on $^{40}\text{Ar}/^{39}\text{Ar}$ geochronology in high-pressure rocks (Sesia-Lanzo Zone, Western Alps), *Geochim. Cosmochim. Acta*, 126, 475–494, 2014.
- Harlov, D. E., Andrut, M., and Pöter, B.: Characterisation of buddingtonite ($\text{NH}_4[\text{AlSi}_3\text{O}_8]$), *Phys. Chem. Min.*, 28, 188–198, 2001.
- Ishizuka, O.: Vertical and horizontal variations of the fast neutron flux in a single irradiation capsule and their significance in the laser-heating $^{40}\text{Ar}/^{39}\text{Ar}$ analysis: Case study for the hydraulic rabbit facility of the JMTR reactor, Japan, *Geochem. J.*, 32, 243–252, 1998.
- Krooss, B. M., Friberg, L., Gensterblum, Y., Hollenstein, J., Prinz, D., and Littke R.: Investigation of the pyrolytic liberation of molecular nitrogen from Palaeozoic sedimentary rocks, *Inter. J. Earth Sci.*, 94, 1023–1038, 2005.
- Lanphere, M. A. and Baadsgaard, H.: Precise K-Ar, $^{40}\text{Ar}/^{39}\text{Ar}$, Rb-Sr and U/Pb mineral ages from the 27.5 Ma Fish Canyon Tuff reference standard, *Chem. Geol.*, 175, 653–671, 2001.
- Laricheva, O. O., Akhmanova, M. V., and Byvkhov, A. M.: Low-temperature hydrothermal synthesis of buddingtonite, *Geochem. Inter.*, 30, 126–132, 1993.
- Loughnan, F. C., Roberts, F. I., and Lindner, A. W.: Buddingtonite (NH_4 -feldspar) in the Condor oilshale deposit, Queensland, Australia, *Mineral. Mag.*, 47, 327–334, 1983.
- Lyckberg, P., Chernousenko, V., and Wilson, W. E.: Famous mineral localities: Volodarsk-Volynski, Zhitomir Oblast, Ukraine, *Mineral. Rec.*, 40, 473–506, 2009.
- Lyckberg, P., Chournousenko, V., and Chournousenko, O.: Giant heliodor and topaz pockets of the Volodarsk chamber pegmatites, Korosten pluton, Ukraine, 36th Intern. Gemmol. Conf., 27–31 August 2019, Nantes, France, 78–83, available at: <https://www.igc-gemmology.org/igc-2019> (last access: 11 January 2022), 2019.
- Mark D. F., Kelley, S. P., Lee, M. R., Parnell, J., Sherlock, S. C., and Brown, D. J.: Ar–Ar dating of authigenic K-feldspar: Quantitative modelling of radiogenic argon-loss through subgrain boundary networks, *Geochim. Cosmochim. Acta*, 72, 2695–2710, 2008.
- Muñoz, J. L. and Eugster, H. P.: Experimental control of fluorine reactions in hydrothermal systems, *Amer. Mineral.*, 54, 943–959, 1969.
- Naumenko-Dèzes, M. O., Villa, I. M., Rolland, Y., Gallet, S., and Lanari, P.: Subgrain $^{40}\text{Ar}/^{39}\text{Ar}$ dating of museum-quality micas reveals intragrain heterogeneity, *Chem. Geol.*, 573, 120215, <https://doi.org/10.1016/j.chemgeo.2021.120215>, 2021.
- Pampeyan, E. H.: Buddingtonite in Menlo Park, California, U.S. Geological Survey Open-File Report 2010-1053, 10 pp., available at: <http://pubs.usgs.gov/of/2010/1053/> (last access: 11 January 2022), 2010.
- Patterson, J. H., Ramsden, A. R., and Dale, L. S.: Geochemistry and mineralogical residences of trace elements in oil shales from the Condor deposit, Queensland, Australia, *Chem. Geol.*, 67, 327–340, 1988.
- Pöter, B., Gottschalk, M., and Heinrich, W.: Crystal-chemistry of synthetic K-feldspar-buddingtonite and muscovite-tobelite solid solutions, *Amer. Mineral.*, 92, 151–165, 2007.
- Rainers, P. W. and Brandon, M. T.: Using thermochronology to understand orogenic erosion, *Ann. Rev. Earth Plant. Sci.*, 34, 419–466, 2006.
- Ramseyer, K., Diamond, L. W., and Boles, J. R.: Authigenic K-NH₄-feldspar in sandstones: A fingerprint of the diagenesis of organic matter, *J. Sedim. Petrol.*, 63, 1092–1099, 1993.
- Renne, P. R., Balco, G., Ludwig, K. R., Mundil, R., and Min, K.: Response to the comment by W. H. Schwarz et al. on “Joint determination of ^{40}K decay constants and $^{40}\text{Ar}^*/^{40}\text{K}$ for the Fish Canyon sanidine standard, and improved accuracy for $^{40}\text{Ar}/^{39}\text{Ar}$ geochronology” by P. R. Renne et al. (2010), *Geochim. Cosmochim. Acta*, 75, 5097–5100, 2011.
- Scibiorski, E., Jourdan, F., Mezger, K., Tohver, E., and Vollstaedt, H.: Cryptic excess argon in metamorphic biotite: Anomalously old $^{40}\text{Ar}/^{39}\text{Ar}$ plateau dates tested with Rb/Sr thermochronology and Ar diffusion modelling, *Geochim. Cosmochim. Acta*, 315, 1–23, 2021.
- Shumlyanskyy, L., Hawkesworth, C., Dhuime, B., Billström, K., Claesson, S., and Storey, C.: $^{207}\text{Pb}/^{206}\text{Pb}$ ages and Hf isotope composition of zircons from sedimentary rocks of the Ukrainian shield: crustal growth of the south-western part of East European craton from Archaean to Neoproterozoic, *Precam. Res.*, 260, 39–54, 2015.
- Shumlyanskyy, L., Nosova, A., Billström, K., Söderlund, U., Andréasson, P.-G., and Kuzmenkova, O.: The U–Pb zircon and baddeleyite ages of the Neoproterozoic Volyn Large Igneous Province: implication for the age of the magmatism and the nature of a crustal contaminant, *Gff Upsala*, 138, 17–30, 2016.
- Shumlyanskyy, L., Hawkesworth, C., Billström, K., Bogdanova, S., Mytrokhyn, O., Romer, R., Dhuime, B., Claesson, S., Ernst, R., Whitehouse, M., and Bilan, O.: The origin of the Palaeoproterozoic AMCG complexes in the Ukrainian shield: New U–Pb ages and Hf isotopes in zircon, *Precam. Res.*, 292, 216–239, 2017.
- Shumlyanskyy, L., Franz, G., Glynn, S., Mytrokhyn, O., Voznyak, D., and Bilan, O.: Geochronology of granites of the western Korosten AMCG complex (Ukrainian Shield): implications for the emplacement history and origin of miarolitic pegmatites, *Eur. J. Mineral.*, 33, 703–716, <https://doi.org/10.5194/ejm-33-703-2021>, 2021.

- Solomon, G. C. and Rossman, G. R.: NH_4^+ in pegmatitic feldspars from the southern Black Hills, South Dakota, *Amer. Mineral.*, 73, 818–821, 1988.
- Steiger, R. H. and Jäger, E.: Subcommission on geochronology: Convention on the use of decay constants in geo- and cosmochronology, *Earth Planet. Sci. Lett.*, 36, 359–362, 1977.
- Svensen, H., Bebout, G., Kronz, A., Li, L., Planke, S., Chevallier, L., and Jamtveit, B.: Nitrogen geochemistry as a tracer of fluid flow in a hydrothermal vent complex in the Karoo Basin, South Africa, *Geochim. Cosmochim. Acta*, 72, 4929–4947, 2008.
- Uto, K., Ishizuka, O., Matsumoto, A., Kamioka, H., and Togashi, S.: Laser-heating $^{40}\text{Ar}/^{39}\text{Ar}$ dating system of the Geological Survey of Japan: System outline and preliminary results, *Bull. Geol. Surv. Japan*, 48, 23–46, 1997.
- Villa, I. M.: Advances in $^{40}\text{Ar}/^{39}\text{Ar}$ Dating: from Archaeology to Planetary Sciences, edited by: Jourdan, F., Mark, D. F., and Verati, C., *Geol. Soc., London, Spec. Pub.*, 378, 107–116, 2014.
- Villa, I. M., De Bièvre, P., Holden, N. E., and Renne, P. R.: IUPAC-IUGS recommendation on the half-life of ^{87}Rb , *Geochim. Cosmochim. Acta*, 164, 382–385, 2015.
- Voncken, J. H. L., Van Roermund, H. L. M., Van der Eerden, A. M. J., Jansen, J. B. H., and Erd, R. C.: Holotype buddingtonite: an ammonium feldspar without zeolitic H_2O , *Amer. Mineral.*, 78, 204–209, 1993.
- Voznyak, D. K., Khomenko, V. M., Franz, G., and Wiedenbeck, M.: Physico-chemical conditions of the late stage Volyn pegmatite evolution: Fluid inclusions in beryl studied by thermobarometry and IR-spectroscopy methods, *Mineral. J. (Ukraine)*, 34, 26–38, 2012.
- Wartho, J., Kelley, S. P., Brooker, R. A., Carroll, M. R., Villa, I. M., and Lee, M. R.: Direct measurement of Ar diffusion profiles in a gem-quality Madagascar K-feldspar using the ultra-violet ablation microprobe (UVLAMP), *Earth Planet. Sci. Lett.*, 170, 141–153, 1999.
- Zhmur, S. I.: Origin of Cambrian fibrous kerites of the Volyn region, *Lithol. Miner. Resour.*, 38, 55–73, 2003.